Cambridge Centre for Computational Chemical Engineering

University of Cambridge

Department of Chemical Engineering

Preprint ISSN 1473 – 4273

Numerical Analysis of a Natural Gas Fuelled HCCI Engine with Exhaust Gas Recirculation, Using a Stochastic Reactor Model

Amit Bhave, Michael Balthasar, Markus Kraft [1], Fabian Mauss [2]

submitted: 5th March 2003

[1] Department of Chemical Engineering
University of Cambridge
Pembroke Street
Cambridge CB2 3RA
UK
E-Mail: markus_kraft@cheng.cam.ac.uk

[2] Division of Combustion Physics
Lund Institute of Technology
Box 118, S-221 00 Lund
Sweden

Preprint No. 8

c4e

Key words and phrases. HCCI combustion and emissions, EGR, Stochastic Reactor Model.

Edited by
Cambridge Centre for Computational Chemical Engineering
Department of Chemical Engineering
University of Cambridge
Cambridge CB2 3RA
United Kingdom.

Fax: + 44 (0)1223 334796
E-Mail: c4e@cheng.cam.ac.uk
World Wide Web: http://www.cheng.cam.ac.uk/c4e/

Abstract

Combustion and emissions formation in a Volvo TD 100 series diesel engine running in a homogeneous charge compression ignition (HCCI) mode and fuelled with natural gas is simulated and compared to experimental measurements for both without and with exhaust gas recirculation (EGR). A new stochastic approach is introduced to model the convective heat transfer, which accounts for fluctuations and fluid-wall interaction effects. This model is included in the Partially stirred plug flow reactor (PaSPFR), a stochastic reactor model (SRM), to study the effect of EGR on pressure, auto-ignition timing and emissions of CO and unburned hydrocarbons (HCs). The model accounts for temperature inhomogeneities and includes a detailed chemical mechanism to simulate the chemical reactions within the combustion chamber. Turbulent mixing is described by the interaction by exchange with the mean (IEM) model. A Monte Carlo method with second order time splitting technique is employed to obtain the numerical solution. The model is validated by comparing the simulated in-cylinder pressure history and emissions, with the measurements taken from the ref.: Christensen, M. *et. al.*, SAE paper 982454. Excellent agreement is obtained between the peak pressure, ignition timing and CO and HC emissions predicted by the model and those obtained from the measurements for the non-EGR, 38% EGR and 47% EGR cases. A comparison between the pressure profiles for the cases studied, reveals that the ignition timing and the peak pressure are dependent on the EGR. With EGR, the peak pressure reduces and the auto-ignition is delayed. The trend observed in the experimentally measured emission values with EGR is also predicted correctly by the model.

Contents

1 Introduction

The homogeneous charge compression ignition (HCCI) engine has attracted a lot of attention in the combustion community for its low NOx emissions and high thermal efficiency characteristics. HCCI engines are a hybrid of spark ignition (SI) and diesel engines. Similar to spark ignition engines, the fuel and air are premixed, but auto-ignition occurs as the in-cylinder charge temperature and the pressure build up due to compression, as is the case with diesel engines. High CO and unburned HC emissions together with the difficulty in starting and controlling the engine are the typical disadvantages of an HCCI engine. If the fuel mixture in the HCCI engine is too rich it can result in a runaway of chemical reactions that can lead to noisy engine operation and in the worst case, engine damage. Therefore, lean mixtures must be used in order to limit the rate of combustion. The dilution can be obtained by high air-fuel ratio (excess air) and/or exhaust gas recirculation (EGR). Due to the lower combustion temperature and reduced oxygen concentration, EGR reduces the combustion rate more than excess air does [3]. On the other hand, if the fuel mixture is too lean, it can lead to a misfire condition. One of the advantages of HCCI is its intrinsic fuel flexibility. Natural gas, propane and gasoline fuels have been successfully used due to their higher octane numbers, enabling higher compression ratios. In particular, for the limited speed and load range requirements of the engine in the stationary engine market, the suitability of natural gas fuelled HCCI engine has been emphasised in [6]. Additionally, the high compression ratios in these engines remove the end gas knock limit that can restrict the SI operation for such a market. In ref. [9], a thorough investigation of natural gas fuelled HCCI technology compared with the available commercial engines in this market is presented. An optimum balance between compression ratio, equivalence ratio and charge dilution by EGR are mentioned to have the potential to improve the HCCI technology.

The experimental research has evolved immensely since the first experimental demonstration of HCCI in a two-stroke engine in 1979 [17]. Several experimental studies on two stroke and four stroke engines performing in HCCI conditions have been carried out, showing the vast potential for further development of HCCI engines. Thring investigated different combinations of EGR and equivalence ratios and suggested an engine concept that uses conventional SI operation at high loads and HCCI operation at part loads [20]. In ref. [3] the influence of different EGR rates, air/fuel ratios and inlet mixture temperatures has been investigated. Recently, the role of air swirl in a directly injected HCCI engine with EGR was studied and the decrease in HC, CO and smoke emissions at injection times earlier or later than optimal was attributed to improved fuel/air mixing [19].

In conjunction with the extensive experimental research, various modelling approaches towards understanding HCCI technology are being developed. The ideal analytical tool would be the combination of a detailed fluid mechanics code and a detailed chemical kinetics model. A direct numerical simulation of this kind would require solving a set of coupled equations, which proves to be computationally prohibitive. A simple, single zone model has been implemented to computationally

study the effect of EGR on combustion rate and its potential for slowing the heat release rate to allow operation at higher fuel loads [4]. In ref. [15], an optimiser has been implemented along with a single zone model to analyse the operating conditions such as EGR, intake pressure, and equivalence ratio for a natural gas fuelled HCCI engine. However, the single zone models (combustion chamber modelled as a plug flow reactor) show discrepancy with measurements for pressure and emissions [2, 10]. This difference in simulation and measurement results can be attributed to the local inhomogeneities. It has been shown that the initial mixture in the cylinder is not homogenous. This is a result of imperfect mixing and the cold mass residing in the crevices and boundary layers, which are too cold to burn to completion. Since the reaction rates are very sensitive to temperature, the consideration of spatial inhomogeneities of temperature in the combustion chamber is crucial for the prediction of pressure and emissions. Multizone models can account for the inhomogeneities by modelling the effects due to thermal boundary layer. Multizone models have been applied to compute NOx and CO emissions for a variety of operating conditions with methane as the fuel. These models, combining fluid mechanics with detailed chemical kinetics are capable of predicting the peak pressures and the CO and HC emissions better than the single zone models [1, 5]. However, these models fail to consider the fluctuations in the zones and the chemical source terms are calculated by using the mean temperature and gas composition in the zones.

A more sophisticated way to account for the inhomogeneities is the use of stochastic reactor models (SRMs) [12]. In such models the assumption of homogeneity within the combustion chamber is replaced by one of statistical homogeneity, with physical quantities being described by a probability density function (PDF) that does not vary within the cylinder. Thus, the spatial distribution of the charge in the cylinder is represented in terms of a PDF. Maigaard *et al.* used such a stochastic equivalent of the classic plug flow reactor (PFR) model, known as the Partially Stirred Plug Flow Reactor (PaSPFR) model to simulate HCCI combustion [12, 14]. In an extension of this work, Kraft *et. al.* demonstrated the use of the PaSPFR model to successfully predict the ignition timing, peak pressure and CO and HC emissions in a HCCI engine and validated the model with the experimental results [13]. The main features of the PaSPFR-IEM (interaction by exchange with the mean) model are that it can account for scalar mixing and fluctuations in quantities, which the multizone models cannot.

In this paper we use the PaSPFR-IEM model to simulate the natural gas fuelled HCCI combustion with EGR. The deterministic approach used in previous works [2, 13, 14] to model the convective heat transfer does not take into account fluctuations. In this paper we introduce a stochastic heat transfer model, based on a Poisson process and Woschni's convective heat transfer coefficient. This model is incorporated into the PaSPFR-IEM model and accounts for fluctuations and fluid-wall interactions. The purpose of this paper is to study the effect of EGR on peak pressure, ignition timing and CO and HC emissions and validate the model predictions against the experimental results taken from ref. [3].

The paper is organized as follows. In the first section, the engine geometry and the operating conditions of the different cases investigated are specified. A brief overview of the measurement techniques from ref. [3] is included. The second section introduces a new stochastic approach to model convective heat transfer and describes the basic features of the stochastic reactor model applied to simulate the combustion and emission formation in the HCCI engine. Finally, the major results of this study related to the validation of the model predictions against the measurements are presented and discussed. Conclusions are drawn in the last section.

2 Experimental description

In this section, a brief overview of the experimental description taken from ref. [3] is included to describe the engine geometry, operating conditions and to compliment the simulation procedure as explained in the next section. A Volvo TD100 series diesel engine was converted to run in HCCI mode. The geometric properties of the test engine are given in **Table 1**.

Table 1: *Volvo TD 100 engine parameters*

Displaced Volume	1600 **cm**^{3}
Bore	120.65 **mm**
Stroke	140 **mm**
Connection Rod	260 **mm**
Exhaust Valve Open	39^0 **BBDC (at** 1 **mm lift)**
Exhaust Valve Close	10^0 **BTDC (at** 1 **mm lift)**
Inlet Valve Open	5^0 **ATDC (at** 1 **mm lift)**
Inlet Valve Close	13^0 **ABDC (at** 1 **mm lift)**

A flat piston crown was used, resulting in a pancake combustion chamber. The inlet mixture was heated with an electric heater. Commercially available natural gas (octane number 120) with a prominent amount of methane was used as fuel. The actual composition of the natural gas is given in **Table 2**. A pressure transducer was mounted in the cylinder head and the cylinder pressure was recorded for 100 cycles, every 0.2 crank angle degrees (CAD).

2.1 Experimental EGR system

To enable the use of EGR, the pressure in the exhaust manifold was increased by throttling the exhaust side. The demerit of this practice is that the pumping work is increased which therefore reduces the efficiency of the engine. The amount of EGR was controlled by a valve in the pipe connecting the inlet and exhaust system. In the

Table 2: *Natural gas components*

Component	**Mole-%**	**Mass-%**
Methane	91.3	81.0
Ethane	5.0	7.9
Propane	1.8	4.3
n-Butane+higher	1.0	4.7
Methane	0.3	0.9
Carbondioxide	0.6	1.2

case of lean mixtures, the molar masses of the fresh mixture and the exhaust gas are the same. Hence, the amount of EGR was evaluated experimentally, by measuring the CO_2 concentration in the inlet and the exhaust. The amount of EGR is defined as

$$\text{EGR} = \frac{\dot{m}_e}{\dot{m}_e + \dot{m}_f + \dot{m}_a} \tag{1}$$

where, $\dot{m}_a$, $\dot{m}_f$ and $\dot{m}_e$ are the mass flow rates of the air, fuel and exhaust gases respectively. Exhaust gas was mixed with the fresh air-fuel mixture, keeping the fuel flow constant, and reducing the quantity of fresh air. Thus with increasing EGR the relative air/fuel ratio (λ) decreases as given in **Table 3**. The temperature to which the mixture is reheated depends on the percentage of EGR. With a higher recirculation of exhaust gases, a higher initial temperature is required to initiate and sustain the chemical reactions leading to auto-ignition. For example as given in **Table 3**, in the non-EGR case the mixture was heated to temperature, $T = 445$ K, at $P = 1$ bar pressure before being fed to the inlet, whereas, with 47% EGR, the mixture was heated to the inlet conditions of $T = 465$ K and $P = 1$ bar pressure.

Table 3: *EGR amounts and corresponding relative air-fuel ratios and temperatures*

EGR (%)	T[**K**]	λ
0	445	3.12
38	455	1.82
47	465	1.51

2.2 Emission Analysis

For the emissions measurements a complete analyzer system capable of measuring HC, CO_2, O_2 and CO was used. The HCs were measured wet, while the other gases were measured dry. The unburned HCs were measured using a Flame Ionisation Detector (FID) that measured in the range 0-100000 ppm. To support the flame a

gas mixture of 60% He and 40% H_2 was needed. CO_2, O_2 and CO were measured using a Non Dispersive InfraRed analyser (NDIR). The CO_2 could be measured in the range $0-16\%$ and O_2 in the range $0-25\%$. The system is equipped with dual CO_2 meters, to be able to measure EGR. CO was measured in two different ranges, $0-2500$ ppm for low concentrations and $0-10\%$ for high concentration. All measurements were taken at a point that corresponds to a crank angle of 180 degrees.

3 Modelling description

The global quantities such as the mass m, volume $V(t)$, mean density $\rho(t)$, and the mean pressure $P(t)$ in the cylinder are assumed to be spatially homogeneous. The volume, $V(t)$, in terms of crank angle degree (CAD), θ, is calculated as:

$$V(t) = V_c + \frac{\pi}{4}B^2(l + a - a\cos\theta + \sqrt{l^2 - a^2\cos^2\theta}) \tag{2}$$

where, V_c is the clearance volume, B the engine bore, l the connecting rod length and a, the ratio of l to the crank radius. The mean density is defined by:

$$\langle\rho(t)\rangle = \frac{m}{V(t)} \tag{3}$$

and the mean pressure is calculated from the equation of state

$$P(t) = \langle\rho(t)\rangle R\frac{\langle T(t)\rangle}{\langle M\rangle} \tag{4}$$

where $\langle T\rangle$ and $\langle M\rangle$ are the mean temperature and expected mean molecular weight.

Local quantities such as mass fractions, $Y_i(t), i = 1,\ldots,S$ and temperature, T(t) are treated as random variables. Let $\phi(t) = (\phi_1,\ldots,\phi_S,\phi_{S+1};t) = (Y_1,\ldots,Y_S,T;t)$, denote the vector containing the random variables. $\psi_1,\ldots,\psi_{S+1}$ are the realisations (sample space variables) of the corresponding random variables $\phi_1,\ldots,\phi_{S+1}$. The time evolution of their joint scalar mass density function (MDF), $\mathcal{F}(\psi_1\ldots,\psi_{S+1};t)$, assuming statistical homogeneity as proposed in the PaSPFR model is given by:

$$\frac{\partial}{\partial t}\mathcal{F}_\phi(\psi,t) + \frac{\partial}{\partial\psi_i}(Q_i(\psi)\mathcal{F}_\phi(\psi,t)) = \frac{\partial}{\partial\psi_i}\left[\frac{C_\phi}{2\tau}(\psi_i - \langle\phi_i\rangle)\mathcal{F}_\phi(\psi,t)\right] \tag{5}$$

with the initial conditions:

$$\mathcal{F}_\phi(\psi,0) = \mathcal{F}_0(\psi). \tag{6}$$

The brackets $\langle.\rangle$ denote the mean according to $\mathcal{F}_\phi$, and $\frac{C_\phi}{\tau}$ is a measure of the intensity of scalar mixing. The interaction by exchange with the mean (IEM) model, explained in [18] is used to describe the mixing of scalars by turbulent diffusion. The R.H.S. of Eq. (5) represents the IEM model. The source term Q_i denotes the change

of the MDF due to chemical reactions, heat losses and change in volume, dV, given by:

$$Q_i = \frac{M_i}{\rho} \sum_{j=1}^{r} \nu_{i,j}\omega_j \quad i = 1, \ldots, S; \tag{7}$$

$$Q_{S+1} = \frac{1}{c_v} \sum_{i=1}^{S} \left(h_i - \frac{RT}{M_i} \right) \frac{M_i}{\rho} \sum_{j=1}^{r} \nu_{i,j}\omega_j + \frac{P}{mc_v}\frac{dV}{dt} - \frac{\alpha\sigma\beta}{\rho c_v}(T^4 - {T_w}^4) - \frac{h_g A}{mc_v}(T - T_w) \tag{8}$$

where, h_i and h_g represent the enthalpy of a species i and Woschni's heat transfer coefficient [8] respectively, T is the mean temperature of the gas, T_w is the cylinder wall temperature and the variable A denotes the heat transfer area. A simple radiation model with an optical thin gas approximation is implemented to calculate heat loss due to radiation. σ is the Stefan-Boltzmann constant, α is the geometry factor and β is the sum of planck absorption coefficients based on CO_2 and H_2O. A detailed chemical mechanism comprising of $r = 857$ chemical reactions and $S = 71$ species is implemented [11, 13].

To obtain the solution of Eq. (5) with the initial conditions given by Eq. (6), a Monte Carlo method with a second order operator splitting technique is employed. The Monte Carlo method involves the approximation of the initial density function by a stochastic particle ensemble of size N

$$\mathcal{F} \approx \mathcal{F}^N = \frac{1}{N} \sum_{n=1}^{N} \delta_{\psi^{(n)}}. \tag{9}$$

Then, the particles in the ensemble are moved according to the evolution of the density function. Each stochastic particle is equi-weighted and has a temperature and a mass, and is thereby related to the fluid particle.

The operator splitting technique can be explained with a flowchart of the sequential steps involved, as shown in the Figure 1. The flowchart (A) in the **Figure 1** shows the splitting algorithm employed in the previous work [13]. With a time marching (time step size: Δt), the mixing step is carried over the whole stochastic particle ensemble for $\Delta t/2$. This is followed by the next step which accounts for the effect of the chemical reactions, change in volume and the heat losses due to convection and radiation, as given in Eq. (8). Lastly the mixing step is performed for $\Delta t/2$. This completes one time advancing loop and the in-cylinder mean temperature, pressure and emissions are calculated from the particle properties at the end of each time step. In this paper, we split the step that accounts for the effect of heat loss due to convection as shown in flowchart (B). The heat loss due to convection event is performed over time step (Δt), after the first mixing step. This event is followed by the step, considering the effect of the chemical reactions, change in volume, and the radiative heat transfer loss, and then the mixing step is performed at the end as in [13].

In the previous work [13, 14] all the particles in the ensemble were moved according to Woschni's heat transfer coefficient, h_g and area, A, to account for the effect of heat loss due to convection. However, the local temperature information attributed to the boundary layer particles is lost due to the instantaneous combustion which induces a need to introduce fluctuations to represent the inhomogeneities due to the colder boundary layer. This is particularly important for the iterative method used for modelling the EGR cases. The fluctuations are introduced by using a stochastic approach for modelling the convective heat transfer event.

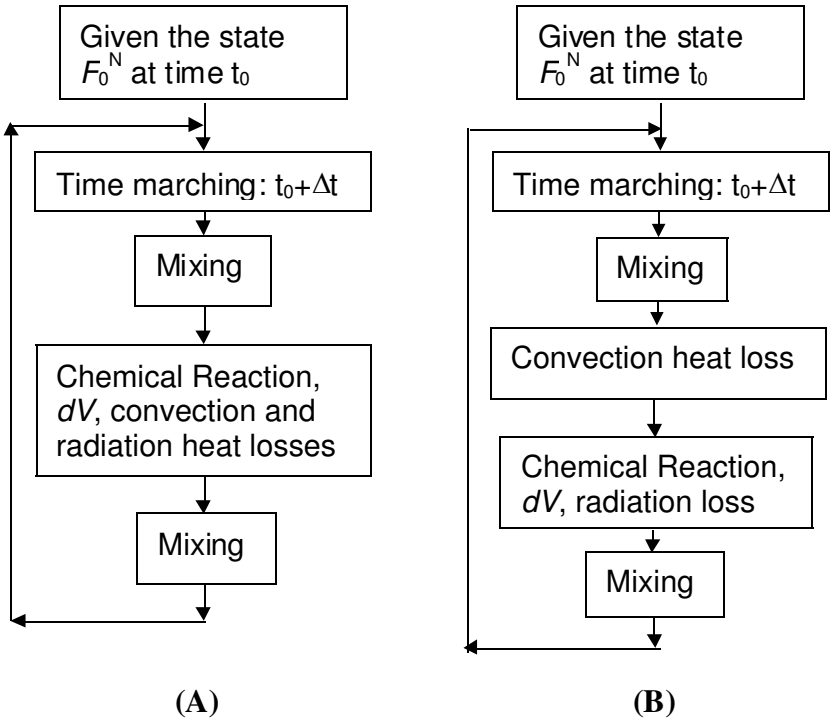

Figure 1: *Time splitting scheme for Monte Carlo particle algorithms.*

Thus, for the present work, we modify Eq. (5):

$$\begin{aligned}\frac{\partial}{\partial t}\mathcal{F}_\phi(\psi,t)+\frac{\partial}{\partial \psi_i}(G_i(\psi)\mathcal{F}_\phi(\psi,t))+\frac{\partial}{\partial \psi_{S+1}}(U(\psi_{S+1})\mathcal{F}_\phi(\psi,t))\\ =\frac{\partial}{\partial \psi_i}\left[\frac{C_\phi}{2\tau}(\psi_i-\langle\phi_i\rangle)\mathcal{F}_\phi(\psi,t)\right]\end{aligned} \tag{10}$$

with the initial conditions:

$$\mathcal{F}_\phi(\psi,0)=\mathcal{F}_0(\psi) \tag{11}$$

where,

$$U = \frac{-h_g A}{c_v m}(T - T_w) \tag{12}$$

$$G_i = \frac{M_i}{\rho}\sum_{j=1}^{r}\nu_{i,j}\omega_j \quad i = 1, \ldots, S \tag{13}$$

$$G_{S+1} = \frac{1}{c_v}\sum_{i=1}^{S}\left(h_i - \frac{RT}{M_i}\right)\frac{M_i}{\rho}\sum_{j=1}^{r}\nu_{i,j}\omega_j + \frac{P}{mc_v}\frac{dV}{dt} - \frac{\alpha\sigma\beta}{\rho c_v}(T^4 - {T_w}^4) \tag{14}$$

Now, to introduce the fluctuations, the third term on L.H.S. of Eq. (10) is replaced by the finite difference scheme:

$$\frac{1}{h}\left[U(\psi_{S+1})\mathcal{F}(\psi, t) - U(\psi_{S+1} - h)\mathcal{F}(\psi_1, \ldots, \psi_S, \psi_{S+1} - h, t)\right], \quad U(\psi_{S+1}) < 0$$

and

$$\frac{1}{h}\left[U(\psi_{S+1})\mathcal{F}(\psi, t) - U(\psi_{S+1} + h)\mathcal{F}(\psi_1, \ldots, \psi_S, \psi_{S+1} + h, t)\right], \quad U(\psi_{S+1}) > 0 \tag{15}$$

where, h is the fluctuation. For the present work, h is a parameter of the model. Ideally the information about h should be obtained from a fluid dynamics code, which is a matter of future work.

The detailed algorithm for incorporating the convective heat transfer step, based on Eq. (10), Eq. (12) and Eq. (15) is explained in next sub-section.

3.1 Heat loss by convection

Equations (10),(12) and (15) determine a Poisson process where a stochastic particle is chosen according to uniform distribution. Then the temperature of the particle changes according to the temperature difference between the particle and the wall and according to fluctuation intensity, h. Physically this is equivalent to a practical case in an engine cylinder, where fluid particles in the bulk can travel to the wall and crevices during the piston movement and get cooled or heated due to the interaction with the wall.

The sample space variable ψ_{S+1} associated with a particle is considered as $T^{(n)}, \quad n = 1, \ldots, N$. The algorithm is implemented within each deterministic time step, such as $t \longrightarrow t + \Delta t$.

1. Determine the state of the system of particles according to MDF, $\mathcal{F}^N(\psi, t)$, at time $t = t_0$
2. Calculate the fluctuation $h^{(n)} = \left|\frac{T^{(n)} - T_w}{C_h}\right|$ for the particles

3. Wait an exponentially distributed time step, $\hat{\tau}$ with parameter

$$\pi(p) = \frac{h_g A C_h N}{m c_v}$$

4. Choose particle index n according to uniform distribution in the interval $[1, N]$

5. Perform temperature jump on the particle with reference to T_w

$$T_{\text{new}}^{(n)} = T^{(n)} + h^{(n)}, \quad T^{(n)} < T_w$$
$$T_{\text{new}}^{(n)} = T^{(n)} - h^{(n)}, \quad T^{(n)} > T_w$$

6. If $t < t_0 + \Delta t$ go to step 2.

The parameter $h^{(n)}$ induces fluctuation and C_h is a parameter in the model which changes the magnitude of the fluctuation.

3.2 Numerical study

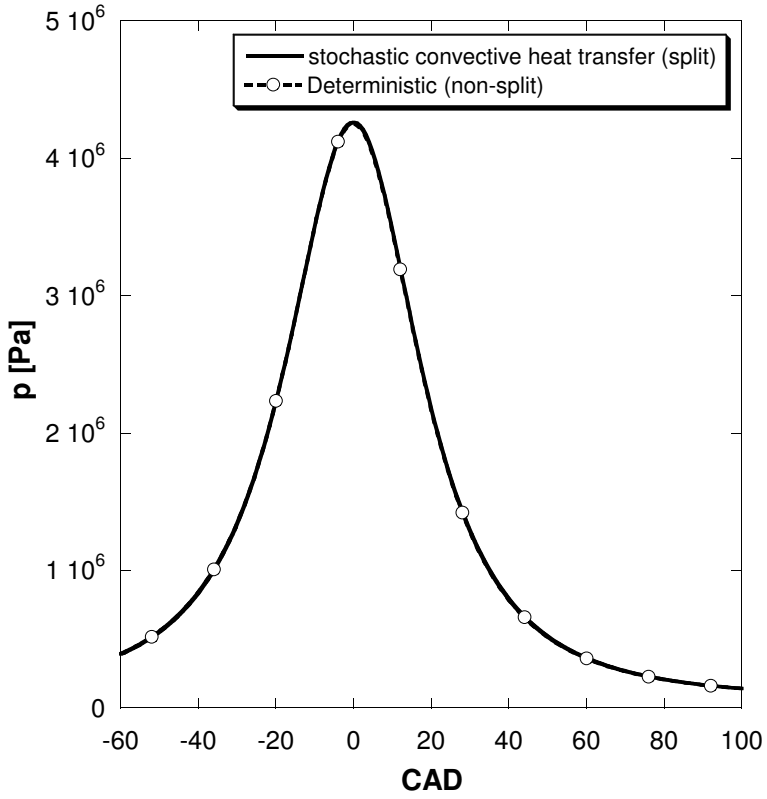

Figure 2: *In-cylinder pressure (excluding the effect of chemical kinetics).*

For the Monte Carlo method with time splitting technique implemented, Δt and N are the two sources of numerical error [18]. **Figure 2** shows the result of a numerical study where the in-cylinder pressure evolution is compared for the algorithms given in **Figure 1**. The effect of chemical kinetics is not included, that is the in-cylinder temperature is affected by the heat losses due to convection and radiation, change in volume, and mixing events. A good agreement is obtained for pressure profiles in the non-split (Flowchart (A)) and split (Flowchart (B), with $h \longrightarrow 0, C_h = 10^9$) algorithms. Thus, there is no appreciable error introduced due to time splitting. Also, this shows that in the limiting case, where the stochastic fluctuations tend to zero the stochastic approach and deterministic approach converge.

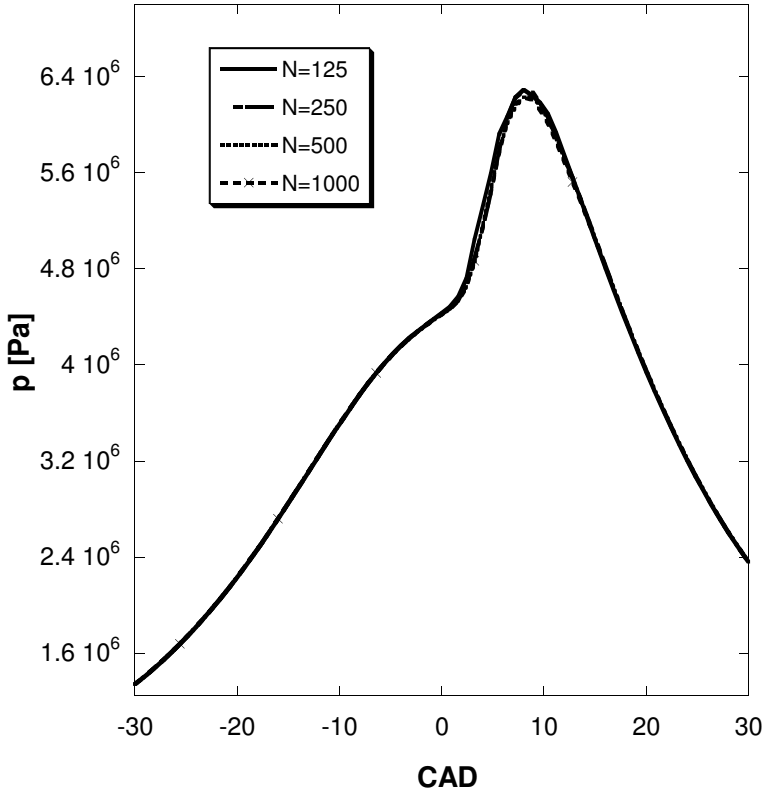

Figure 3: *In-cylinder pressure with increasing N.*

Increasing the number of particles, N, decreases the numerical error. However, an increase in N also increases the computational expense in terms of CPU time. For a simulation with 125 stochastic particles, the CPU time required was about 55 minutes as compared to 8 hours required for, $N = 1000$ particles on a PIII 866 MHz PC. Figure 3 illustrates that a choice of $N = 125$ particles is sufficient to achieve an acceptable accuracy in the pressure profiles.

3.3 Simulation procedure

Throughout the simulation study, number of particles, $N = 125$ and the fluctuation parameter, C_h is set at 50. To account for the local temperature inhomogeneities, a colder thermal boundary layer was considered close to the cylinder surface. As explained in [7, 8], approximately 80% of the gas mixture resides in the bulk of the cylinder and 20% in the boundary layer. The temperature distribution in the thermal boundary layer was modelled as mentioned in [13] for the non-EGR case only. For EGR case, the initial temperature profile of the particles is affected by the EGR temperature. The initial values for simulating the non-EGR case were used as given in **Table 4**.

Table 4: *Initial values for the simulations [0% EGR] (60 CAD BTDC)*

CR	T**[K]**	P**[bar]**	**RPM**
18	630	3.988	1000

From non-EGR to EGR cases, only the operating conditions such as the relative air-fuel ratio, λ and the temperature, T were changed as given in **Table 3**. Note that the stochastic fluctuation along with rest of the model parameters from the non-EGR case, were kept constant while modelling the EGR cases. In order to include EGR in the simulations, the exhaust gas composition is stored and is first cooled down to room temperature ($T = 298$K) and $P = 1$ bar using an equilibrium code, before being mixed with air and fuel (according to the EGR definition). The mixture is then reheated to temperature and pressure, corresponding to the amount of EGR (38% or 47%). The code is then re-run with the new composition of the inlet mixture. This procedure is repeated until convergence is obtained. Normally, $4 - 5$ iterations were found to be necessary to obtain the convergence of the peak pressure.

4 Results and discussion

The pressure profiles and the emissions for the non-EGR, 38% EGR and the 47% EGR cases are discussed and a comparison is made with the experimental results.

4.1 Pressure

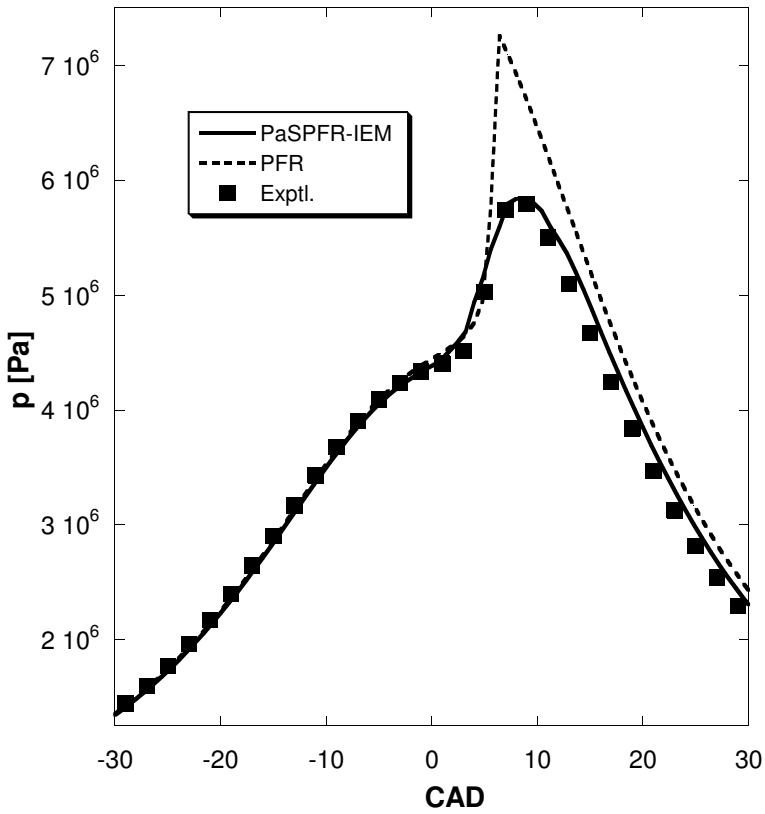

Figure 4: *Pressure profile: Results from PaSPFR-IEM model compared to experimental results (taken from ref. [3]) and results obtained from a homogeneous reactor model for non-EGR case.*

With the PaSPFR model implemented, the pressure prediction is validated by comparing the pressure profile with the experimentally measured pressure in the cylinder. For the non-EGR case an excellent agreement is obtained between the results predicted by the PaSPFR-IEM model and the measurements for the auto-ignition timing and the peak pressure (**Figure 4**). The PaSPFR-IEM model also outperforms the homogeneous - plug flow reactor (PFR) model as the PFR model overpredicts the peak pressure due to its inability to account for local inhomogeneities arising due to the boundary layer effects. For 38% as well as 47% EGR cases, a good agreement is obtained between the model and the measurements for the peak pressure and the ignition timing predictions as shown in **Figure 5**.

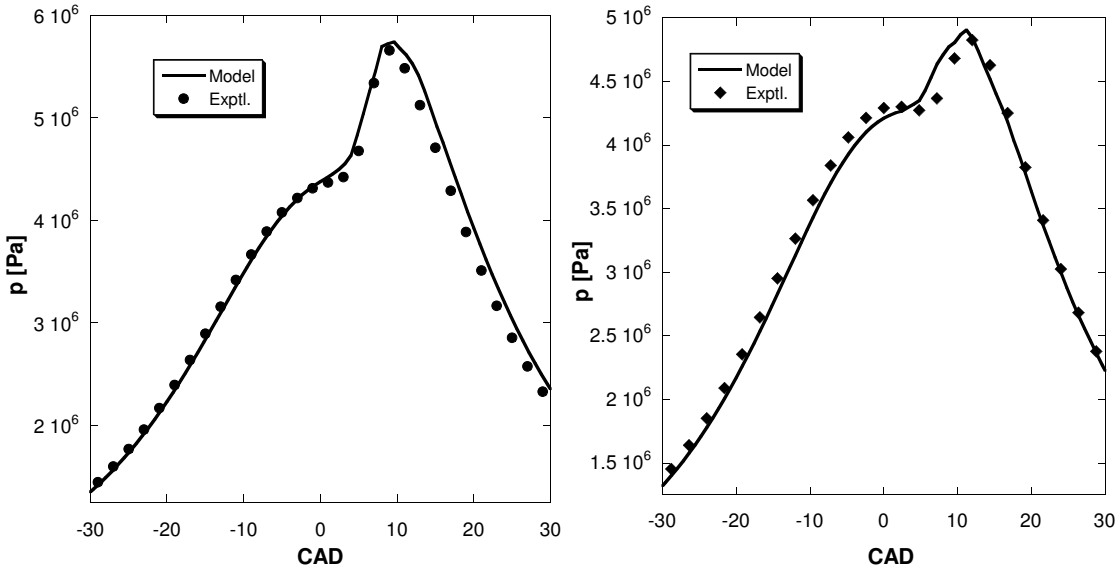

(a) 38%EGR (b) 47%EGR

Figure 5: *Pressure profile: Results from PaSPFR model compared to experimental results (taken from ref. [3]) for* 38% *and* 47% *EGR cases.*

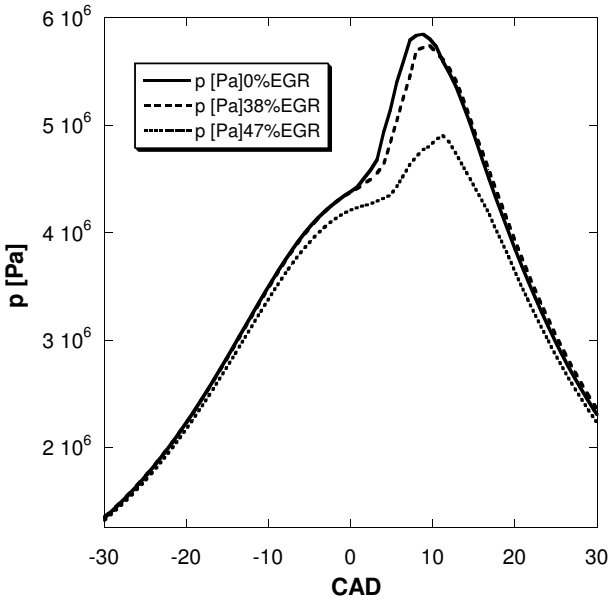

Figure 6: *In-cylinder pressure variation with the EGR amount. Results from PaSPFR model for non-EGR,* 38% *EGR and* 47% *EGR.*

As depicted in **Figure 6**, a decrease in peak pressure and a delay in the auto-ignition timing with increase in the EGR amount are correctly predicted by the model. The

ratio of specific heats for EGR is lower than that of air. Thus EGR reduces the compressed gas temperature, which retards the combustion timing and slows down the reaction rate in agreement with the results in refs. [4, 16] . The charge heating effect due to EGR as explained in [21] does not play a vital role, since the exhaust gases are cooled down to room temperature before mixing them with the fresh air-fuel mixture. The sensitivity of the peak pressure on changes in the initial bulk temperature was found to be very high. Thus, a precise knowledge of the inlet temperature is vital in predicting the peak pressures under the conditions studied here.

4.2 CO and HC emissions

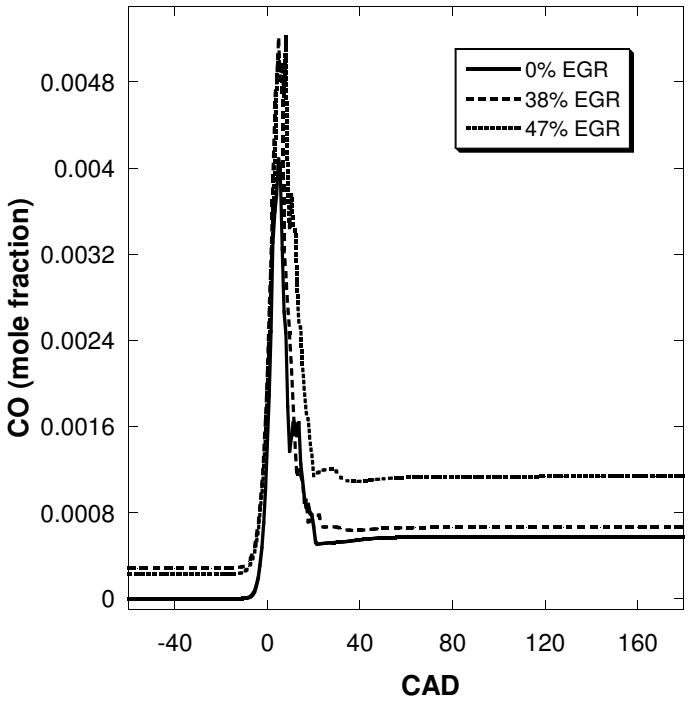

Figure 7: *Variation in CO-emissions with amount of EGR. Results from PaSPFR model for non-EGR,* 38% *EGR and* 47% *EGR.*

As shown in **Figure 7**, the trend observed in the experimental values, i.e., an increase in CO in the exhaust with increasing EGR amount is correctly predicted by the model.

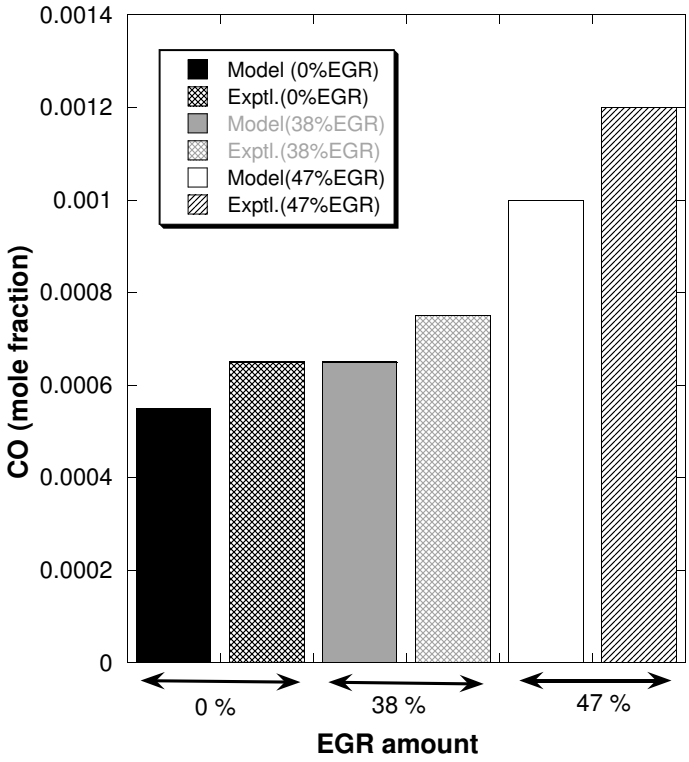

Figure 8: *CO-emissions. Results from PaSPFR model compared to exhaust measurements (taken from ref. [3]) for non-EGR, 38% EGR and 47% EGR.*

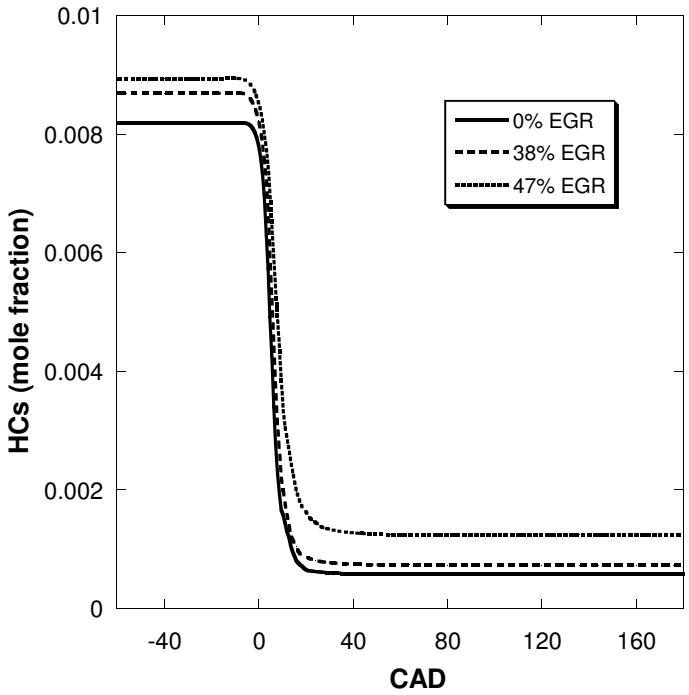

Figure 9: *Variation in HC-emissions with amount of EGR. Results from PaSPFR model for non-EGR, 38% EGR and 47% EGR.*

A comparison between computed CO mole fractions and measured exhaust values is presented in **Figure 8**. In the case of non-EGR, the CO emissions are predicted well, and are 80% of the experimental values. The sharp rise in the CO mole fraction represents the burning of the bulk fuel-air mixture, where maximum CO is produced; this is further oxidised resulting in a lower steady state value. The major source of CO can be attributed to the incomplete combustion of the colder boundary particles due to the freezing of reactions at low temperature and pressure. For the 38% and 47% EGR cases, the CO emissions are predicted with the same accuracy.

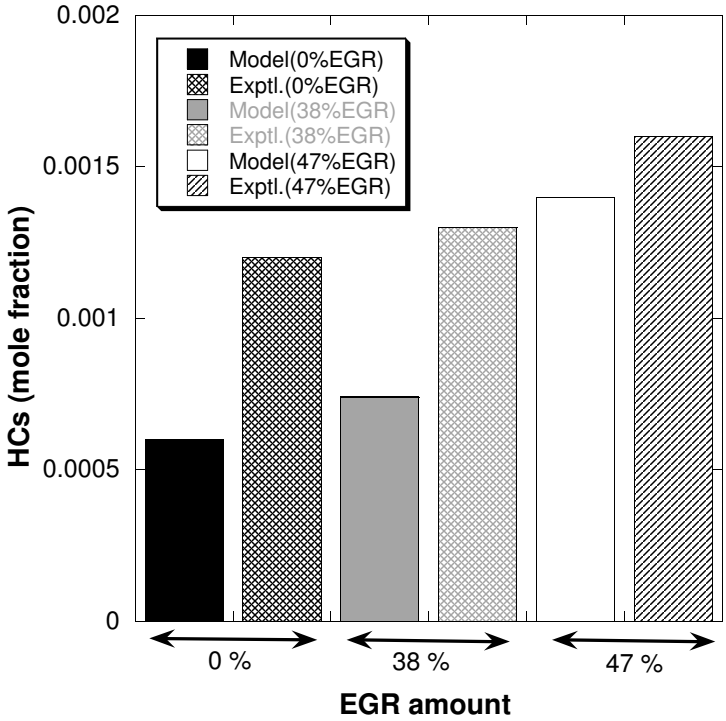

Figure 10: *HC-emissions. Results from PaSPFR model compared to exhaust measurements (taken from ref. [3]) for non-EGR,* 38% *EGR and* 47% *EGR.*

With increasing EGR amount, the HC emissions increased as observed in the experiments (**Figure 9**). The HC emissions predicted by the PaSPFR model and those measured in the experiments are shown in **Figure 10**. For the non-EGR and 38% EGR cases, the amount of unburned hydrocarbons (HCs) predicted by the model was about 60% of the experimental value. With 47% EGR, the model predicted 80% of the HC emissions measured.

5 Conclusions

The compression of the air-fuel mixture by the piston and the combustion process in an HCCI engine fuelled with natural gas, with and without EGR are modelled using

a PaSPFR-IEM model. A detailed chemical mechanism is used to describe ignition, combustion and emission formation. A new approach based on a Poisson process was introduced for modelling the heat transfer by convection. This approach has the advantage that the fluctuations caused by the fluid-wall interaction effects can be accounted.

enabled better accounting for fluctuations and modelling of the particle-wall interaction effects than a deterministic approach. The in-cylinder pressure and the emissions predicted by the model were validated against the experimental results.

In case of 0% EGR, the ignition time and the peak pressure are predicted correctly for conditions different from those mentioned in [12], thus proving the robustness of the PaSPFR-IEM model. The CO and HC emissions are predicted well in comparison with the experimental values.

EGR reduces the compressed gas temperature, thereby retarding the combustion timing and slowing down the reaction rate. With EGR, a good agreement between the model and the measurements for the peak pressure, auto-ignition timing and CO and HC emissions was obtained. The trends observed in the measured CO and HC emissions for non-EGR, 38% EGR and 47% EGR were also correctly predicted by the model.

A full engine cycle simulation directly computes the gas exchange thus proving more advantageous than a closed volume model. Future development of the work will be the full engine cycle simulation for different fuels, by coupling the PDF-based stochastic reactor model with a fluid dynamics code in order to address global engine performance parameters as well as the combustion parameters.

6 Acknowledgements

The authors gratefully acknowledge the financial support from the Cambridge Commonwealth Trust, Overseas Research Studentship (ORS) committee (AB), the EPSRC grant number GR/R53784 (MK), and The Royal Society and Churchill College, Cambridge (MB). The authors thank Magnus Christensen and Bengt Johansson (Lund Institute of Technology) for the help and discussions related to the measurements.

7 Nomenclature

A	Cylinder surface area
a	Crank radius
ABDC	After Bottom Dead Centre
ATDC	After Top Dead Centre
B	Cylinder bore
BBDC	Before Bottom Dead Centre
BTDC	Before Top Dead Centre
CAD	Crank angle degree
CR	Compression ratio
c_v	Heat capacity at constant volume
C_ϕ	Proportionality constant
C_h	Stochastic fluctuation parameter
EGR	Exhaust Gas Recirculation
h	Stochastic fluctuation
HCCI	Homogeneous Charge Compression Ignition
h^n	Stochastic fluctuation for a particle n
h_g	Woschni's convective heat transfer coefficient
h_i	Specific enthalpy of species i
IEM	Interaction by Exchange with the Mean
l	Connecting rod length
m	Total mass
$\langle M \rangle$	Expected mean molecular weight
MDF	Mass Density Function
N	Number of stochastic particles
n	Particle index
P	In-cylinder pressure
PaSPFR	Partially Stirred Plug Flow Reactor
PDF	Probability Density Function
PFR	Plug Flow Reactor
R	Gas constant
r	Number of chemical reactions
S	Chemical species
SRM	Stochastic Reactor Model

T	Flow temperature
T_w	Wall temperature
V	In-cylinder volume
V_c	Clearance volume
Y_i	Mass fraction of species i

Greek symbols

λ	Relative air-fuel ratio
θ	Crank angle degrees
δ	Dirac delta function
ρ	Density
ϕ	Vector of random variables
ψ	Vector of sample space variables
τ	Characteristic mixing time
ω	chemical source term
Δt	Global deterministic time step
$\hat{\tau}$	Waiting time parameter

References

[1] Aceves, S., Flowers, D., Westbrook, C., Smith, J., Pitz, W., Dibble, R., M., C. and B., J. (2000). A multi-zone model for predictions of HCCI combustion and emissions, *SAE 2000-01-0327*.

[2] Amnéus, P., Nilsson, D., Mauss, F., Christensen, M. and Johansson, B. (1998). Homogeneous charge compression ignition engine: Experiments and detailed kinetics calculation, *Comodia 98*.

[3] Christensen, M. and Johansson, B. (1998). Influence of mixture quality on homogeneous charge compression ignition, *SAE 982454*.

[4] Dec, J. E. (2002). A computational study of the effect of low fuel loading and EGR on heat release rates and combustion limits in HCCI engines, *SAE 2002-01-1309*.

[5] Easley, W. L., Agarwal, A. and Lavoie, G. A. (2001). Modelling of HCCI combustion and emissions using detailed chemistry, *SAE 2001-01-1029*.

[6] Fiveland, S. B., Agama, R., Christensen, M., Johansson, B., Hiltner, J., Mauss, F. and Assanis, D. N. (2001). Experimental and simulated results detailing the sensitivity of natural gas HCCI engines to fuel composition, *SAE 2001-01-3609*.

[7] Fiveland, S. B. and Assanis, D. N. (2001). Development of a two zone HCCI combustion model accounting for boundary layer effects, *SAE 2001-01-1028*.

[8] Heywood, J. B. (1988). *Monte Carlo Methods*, 1st edn, McGraw-Hill publications, New York, p. 680.

[9] Hiltner, J., Fiveland, S. B., Agama, R. and Willi, M. (2002). System efficiency issues for natural gas fueled HCCI engines in heavy-duty stationary applications, *SAE 2002-01-0417*.

[10] Kelly-Zion, P. L. and Dec, J. E. (2000). A computational study of the effect of fuel type on ignition time in homogeneous charge compression ignition engines, *Proc. Comb. Inst.* **28**: 1187–1195.

[11] Klaus, P. (1998). *PhD Thesis: Entwicklung eines detaillierten Reaktionsmechanismus zur Model-lierung der Bildung von Stickoxiden in Flammenfronten*, IWR Heidelberg, Department of Physical Chemistry.

[12] Kraft, M. (1998). *Stochastic Modelling of Turbulent Reacting Flow in Chemical Engineering*, number 391 in *Fortschrittsberichte des VDI, Reihe 6*, 1st edn, Düsseldorf: VDI Verlag.

[13] Kraft, M., Maigaard, P., Mauss, F., Christensen, M. and Johansson, B. (2000). Investigation of combustion emissions in a homogeneous charge compression ignition engine: Measurements and a new computational model, *Proc. Comb. Inst.* **28**: 1195–1201.

[14] Maigaard, P., Mauss, F. and Kraft, M. (2000). Homogeneous charge compression ignition engines: A simulation study on the effect of inhomogeneities, *ASME 2000-ICE-275*.

[15] Martinez-Frias, J., Aceves, S. M., Flowers, D. and Smith, J. R. (2001). Equivalence ratio - EGR control of HCCI engine operation and the potential for transition to spark - ignited operation, *SAE 2001-01-3613*.

[16] Nakano, M., Mandokoro, Y., Kubo, S. and Yamazaki, S. (2000). Effects of exhaust gas recirculation in homogeneous charge compression ignition engines, *Int. J. Engine. Research.* **1**(3): 269–279.

[17] Onishi, S., Jo, S. H., Shoda, K., Jo, P. D. and Kato, S. (1979). Active thermo-atmospheric combustion (ATAC) - a new combustion process for internal combustion engines, *SAE 790501*.

[18] Pope, S. B. (1985). Pdf methods for turbulent reactive flows, *Energy Combust. Sci.* **11**: 119–192.

[19] Sjöberg, M., Edling, L., Eliassen, T., Magnusson, L. and Angström, H. (2002). GDI HCCI: Effects of injection timing and air swirl on fuel stratification, combustion and emissions formation, *SAE 2002-01-0106*.

[20] Thring, R. H. (1989). Homogeneous charge compression ignition (HCCI) engines, *SAE 892068*.

[21] Zhao, H., Peng, Z., Williams and J., Ladommatos, N. (2001). Understanding the effects of recycled burnt gases on the controlled autoignition (CAI) combustion in four-stroke gasoline engines, *SAE 2001-01-3607*.